Granulocytes in Ocular HSV-1 Infection: Opposing Roles of Mast Cells and Neutrophils

Derek J. Royer,[1] Min Zheng,[2] Christopher D. Conrady,[1] and Daniel J. J. Carr[1,2]

[1]Department of Microbiology and Immunology, The University of Oklahoma Health Sciences Center, Oklahoma City, Oklahoma, United States
[2]Department of Ophthalmology, The University of Oklahoma Health Sciences Center, Oklahoma City, Oklahoma, United States

Correspondence: Daniel J. J. Carr, Department of Ophthalmology, DMEI Pavilion A, Room 415, 608 Stanton L. Young Boulevard, Oklahoma City, OK 73104, USA; Dan-Carr@ouhsc.edu.

Submitted: March 18, 2015
Accepted: April 23, 2015

Citation: Royer DJ, Zheng M, Conrady CD, Carr DJJ. Granulocytes in ocular HSV-1 infection: opposing roles of mast cells and neutrophils. *Invest Ophthalmol Vis Sci*. 2015;56:3763–3775. DOI:10.1167/iovs.15-16900

Purpose. The contributions of mast cells (MCs) to immunologic defense against pathogens in the eye are unknown. We have characterized pericorneal MCs as tissue-resident innate sentinels and determined their impact on the immune response to herpes simplex virus type-1 (HSV-1), a common ocular pathogen.

Methods. The impact of mast cells on the immune response to HSV-1 infection was investigated using MC-deficient $Kit^{W\text{-}sh}$ mice. Virus titers, inflammatory cytokine production, eicosanoid profiles, cellular immune responses, and ocular pathology were evaluated and compared with C57BL/6J mice during an acute corneal HSV-1 infection.

Results. Corneas of $Kit^{W\text{-}sh}$ mice have higher viral titers, increased edema, and greater leukocyte infiltration following HSV-1 infection. Following infection, cytokine profiles were slightly elevated overall in $Kit^{W\text{-}sh}$ mice. Eicosanoid profiles were remarkably different only when comparing uninfected corneas from both groups. Neutrophils within infected corneas expressed HSV-1 antigen, lytic genes, and served as a disease-causing vector when adoptively transferred into immunocompromised animals. Myeloid-derived suppressor cells did not infiltrate into the cornea or suppress the expansion, recruitment, or cytokine production by $CD8^+$ T cells following acute HSV-1 infection.

Conclusions. Collectively, these findings provide new insight into host defense in the cornea and the pathogenesis of HSV-1 infection by identifying previously unacknowledged MCs as protective innate sentinels for infection of the ocular surface and reinforcing that neutrophils are detrimental to corneal infection.

Keywords: mast cell, herpes simplex virus type-1, innate immunity, cornea

Herpes simplex virus type-1 (HSV-1) is a neurotropic double-stranded DNA virus with significant clinical interest due to its endemic nature, life-long persistence, and status as the leading cause of infectious corneal blindness.[1,2] The global burden of corneal HSV-1 infection is estimated to be 1.5 million annual occurrences including 40,000 new cases of severe monocular visual impairment or blindness.[3] More than 60% of the human population is infected with and harbors latent HSV-1 in neuronal ganglia.[2,4,5] Periodic reactivation of HSV-1 facilitates shedding of infectious progeny in external mucosae innervated by infected neurons, often resulting in herpes labialis (i.e., cold sores) or ocular herpes keratitis.[2,6] Farooq et al.[7] have reviewed the mechanisms of HSV-1 cell entry and spread in the eye. Intermittent but recurrent HSV-1 reactivation in the cornea contributes to the development of herpes stromal keratitis (HSK), a blinding immunopathology characterized by inflammation, scarring, and neovascularization.[2,3] Investigating processes of immune surveillance and innate countermeasures during the earliest stages of infection is important to better understand HSV-1 pathogenesis, focus development of novel therapeutics, and ultimately prevent HSK.

The innate immune response to HSV-1 infection in the cornea is multifactorial. It is abundantly clear that type-1 IFN-α/β signaling in both resident cells and infiltrating leukocytes is required for control of HSV-1.[8] Due to the avascular nature of the normal cornea, circulating leukocytes must extravasate from blood vessels surrounding the cornea in the limbus and migrate through the tissue in accordance with the local milieu of inflammatory mediators (i.e., cytokines, chemokines, eicosanoids, etc.) following injury or pathogenic insult.[9–12] Acute corneal HSV-1 infection provokes a potent influx of innate leukocytes including inflammatory monocytes, macrophages, natural killer (NK) cells, and neutrophils (PMNs). Of these responders, inflammatory monocytes contribute to virus clearance during the first 48 hours post infection (pi).[8] Conversely, current evidence suggests that PMNs are not responsible for HSV-1 clearance.[13,14] Resident and perhaps infiltrating dendritic cells also respond to HSV-1 infection or regulate the activity of other leukocytes in the cornea.[15]

In addition to resident dendritic cells, an often overlooked bone marrow–derived cell residing in the mucosa of the external eye is the mast cell (MC).[16] Mast cells are long-lived radioresistant granulocytes strategically localized in tissues exposed to the external environment to facilitate pathogen surveillance.[17,18] Mast cells express an armament of innate sensors to accommodate this protective role.[18] Upon stimulation, MCs undergo rapid degranulation of cytoplasmic granules containing preformed proteases and potent vasoactive mediators including histamine and TNFα. Following degranulation, MCs produce many soluble factors de novo to fine-tune subsequent innate and adaptive

responses.[17,18] The scope and functional diversity of immunomodulatory mast cell granule products have recently been reviewed by Wernersson and Pejler.[19]

Though the activities attributed to MCs in general are broad, it is recognized that the MC phenotype and products are regulated in a niche- and stimulus-specific manner.[19,20] Mast cells have been implicated in the maintenance of immune privilege and contribute to pathogen surveillance and defense in various anatomic sites including the skin, lung, bladder, and gut.[18,19,21,22] In the human host, MCs reside in an organized fashion within the eye-associated lymphoid tissue including the lacrimal gland, limbus, and conjunctiva.[23–25] Whereas the contributions of ocular MCs are appreciated in IgE-mediated allergic conjunctivitis, they have not been investigated with respect to pathogen defense in the eye.

In the present article, we hypothesized MCs are involved in the innate immune response to ocular HSV-1 infection due to their proximity to the cornea and immunomodulatory potential. Mice deficient in MCs were found to be more sensitive to HSV-1 infection, but counterintuitively exhibited greater corneal edema. Collectively, our results underscore a novel role for MCs in the eye as an innate sentinel against acute HSV-1 infection by promoting virus clearance and limiting inflammation to preserve the visual axis. We also found that MCs serve as a type of gatekeeper in the corneal vasculature. Imbalances in eicosanoid mediators are implicated in increased corneal PMN infiltration and inflammation in $Kit^{W\text{-}sh}$ mice. Neutrophils were identified as surrogates for HSV-1 replication using in vivo, in vitro, and adoptive cell transfer approaches. Lastly, we establish that myeloid-derived suppressor cells (MDSC) do not compromise the use of $Kit^{W\text{-}sh}$ mice in our model investigating the impact of MCs on the innate and early adaptive immune response to acute HSV-1 infection.

Materials and Methods

Mice and Virus

C57BL/6J wild-type (WT) and C57BL/6J background MC-deficient $Kit^{W\text{-}sh}$ mice were purchased from the Jackson Laboratory (Bar Harbor, ME, USA) and housed at the Dean McGee Eye Institute (DMEI; Oklahoma City, OK, USA) or the O'Donoghue Research Building at the University of Oklahoma Health Sciences Center (OUHSC; Oklahoma City, OK, USA) alongside $CD118^{-/-}$ mice deficient in the IFN-α/β receptor. $CD118^{-/-}$ mice were rederived by the Jackson Laboratory on the C57BL/6J background and genotyped prior to use. Mice were anesthetized and subsequently euthanized via cardiac perfusion with 10 to 15 mL 1× PBS. Animal experiments were conducted in accordance with the ARVO Statement for the Use of Animals in Ophthalmic and Vision Research and the National Institute of Health Guidelines on the Care and Use of Laboratory Animals. Experimental procedures were approved by Institutional Animal Care and Use Committees at DMEI and OUHSC. Herpes simplex virus type-1 strain McKrae was propagated on (CCL)–81 Vero cells (ATCC, Manassas, VA, USA), isolated and pelleted by multistep centrifugation, resuspended in 1× PBS, and stored frozen in aliquots at −80°C.

Reagents

All reagents were purchased from Sigma-Aldrich Corp. (St. Louis, MO, USA) or Fisher Scientific (Waltham, MA, USA), including Triton X-100, paraformaldehyde (PFA), EDTA, heparin, histamine, bovine serum albumin (BSA), methylcellulose, and collagenase type IA (from *Clostridium histolyticum*) unless indicated otherwise. Reagents were certified for molecular biology use or filtered in suspension with a Millex 0.1-μm polyvinylidene fluoride (PVDF) syringe cartridge (EMD Millipore, Billerica, MA, USA) prior to use.

In Vivo HSV-1 Infection

Six- to 12-week-old male and female mice were anesthetized via an intraperitoneal injection of ketamine (100 mg/kg) and xylazine (6.6 mg/kg). The corneal epithelium was partially debrided with a 25-G needle and blotted to remove tear film prior to application of virus. Herpes simplex virus type-1 McKrae was topically applied to each cornea at an inoculum of 1000 plaque forming units (PFU) in 3 μL 1× PBS.

Plaque Assays

Tissues from infected mice were harvested at indicated times pi, suspended in RPMI 1640 media supplemented with 10% FBS, gentamicin, and antibiotic/antimycotic (i.e., normal media; Invitrogen, Grand Island, NY, USA), and processed for 20 to 30 seconds with a Tissuemiser homogenizer (Fisher Scientific). Samples were spun at 10,000*g* for 1.5 minutes and supernatants were serially diluted on monolayers of confluent Vero cells. After 1 hour, monolayers were washed with sterile 1× PBS and replaced with normal media containing 0.5% methylcellulose (Sigma-Aldrich Corp.). Plaques were enumerated 24 to 36 hours later with the aid of a Zeiss inverted microscope (Thornwood, NY, USA).

Corneal Pachymetry

Cornea thickness was measured using a Corneo-Gage Plus digital pachymeter (Sonogage, Cleveland, OH, USA) according to the manufacturer's instructions. Briefly, the 50-MHz probe was delicately held in contact with the central cornea of anesthetized mice so that five consecutive 1000-scan average measurements could be made without interruption. The lowest of the middle three readings was recorded for each cornea analyzed, as this reportedly denotes the measurement most perpendicular to the central cornea.

Microscopy

For all images of corneolimbal whole-mounts, tissue was recovered from euthanized mice, fixed for 30 minutes in 4% PFA in 1× PBS, washed three times for 15 minutes in 1% Triton X-100 in 1× PBS, and labeled via immunohistochemistry, washing in between primary and secondary antibodies. Antibodies were purchased from Abcam (Cambridge, MA, USA), Dako (Carpinteria, CA, USA), EMD Millipore or Jackson ImmunoResearch (West Grove, PA, USA). Mast cell granules were directly stained by FITC-conjugated avidin (Biolegend, San Diego, CA, USA) in fixed tissue as described by Tharp et al.[26] Imaging was performed using the following microscopes: Olympus FV500 confocal, Olympus MacroView MVX10 epifluorescent, and Olympus IX71 for bright-field imaging (Center Valley, PA, USA).

Flow Cytometry and Cell Isolation

Corneas were harvested from euthanized mice at the indicated times pi and digested in 1 mg/mL type 1 collagenase in normal media at 37°C. Samples were triturated every 15 minutes by pipetting for approximately 2 to 2.5 hours. Trigeminal ganglia (TG) were surgically removed and a single cell homogenate was generated in normal media using a Dounce homogenizer (Fisher Scientific). Cornea and TG homogenates were subsequently filtered through 40 μM mesh, washed, and either labeled for flow cytometric analysis or fractionated using Macs immunomagnetic bead technology (Miltenyi Biotec, Bergish Gladbach, Germany) according to the manufacturer's instructions for further downstream applications. Spleens were

Investigative Ophthalmology & Visual Science

Table 1. Primer Sequences of Genes Examined by Quantitative Real-Time PCR

Target Gene	Primer Sequence
β-Actin	5′-CTTCTACAATGAGCTGCGTGTG-3′ (S)
	5′-TTGAAGGTCTCAAACATGATCTGG-3′ (AS)
IFN-β	5′-CAAGAGGAAAGATTGACGTGG-3′ (S)
	5′-TAAGGTACCTTTGCACCCTCC-3′ (AS)
HSV-1 TK	5′-ATACCGACGATCTGCGACCT-3′ (S)
	5′-TTATTGCCGTCATAGCGCGG-3′ (AS)

AS, antisense; S, sense.

removed, punctured, and teased into a single-cell suspension prior to red cell lysis in ammonium chloride and filtration through 70-μM mesh, washed, and labeled for flow cytometry or cultured in vitro. Antibodies for flow cytometry were purchased from eBioscience (San Diego, CA, USA), BD Biosciences (San Jose, CA, USA), or AbD Serotec (Raleigh, NC, USA). Cells were labeled with antibody in the presence of normal rat serum (Jackson ImmunoResearch) following incubation with anti-CD16/32 Fc block, washed twice with 1% BSA in 1× PBS, fixed in 1% PFA, and resuspended in wash buffer for analysis. Neutrophil viability was evaluated using the Miltenyi Biotec annexin V-FITC kit according to the manufacturer's directions. For enumeration and characterization of circulating PMN, 100 μL peripheral blood was collected from the submandibular vein per mouse, mixed with 5 μL 0.5 M EDTA to prevent coagulation, and treated with red blood cell lysis solution (Miltenyi Biotec) according to the manufacturer's instructions prior to downstream applications. For functional assays, cells were labeled intracellularly using the BD Biosciences Cytofix/Cytoperm Plus kit containing Monensin. Samples were analyzed using a MacsQuant flow cytometer and MacsQuantify software (Miltenyi Biotec).

Concanavalin A Perfusion

For limbal leukostasis experiments, mice were euthanized by cardiac perfusion with 15 mL 1× PBS containing 0.1 mg/mL heparin using a ThermoScientific FH10 peristaltic pump (Waltham, MA, USA). Perfusion was continued with 15 mL each of 2% PFA in 1× PBS, 1× PBS, 1% BSA in 1× PBS, 1× PBS containing 20 μg/mL Concanavalin A: FITC (Vector Labs, Burlingame, CA, USA), and 1% BSA in 1× PBS consecutively as previously described.[27] Corneolimbal whole-mounts were then harvested in low-light conditions, fixed for 30 minutes in 4% PFA in 1× PBS, washed, and imaged. Leukocyte adhesion was quantified using ImageJ software (http://imagej.nih.gov/ij/; provided in the public domain by the National Institutes of Health, Bethesda, MD, USA). Briefly, images were reduced to 8-bit, the threshold was auto-adjusted using triangle over/under processing for dark backgrounds, then the leukocytes were counted in the limbus of corneolimbal whole-mounts using the 'analyze particles' function on the resulting binary image. Parameters for the analyze particles function were set as follows: size, 0 to ∞; circularity, 0.3 to 0.99; show outlines.

RNA Array and RT-PCR

A Panomics QuantiGene Plex 2.0 custom multiplex assay (Affymetrix, Santa Clara, CA, USA) was used to evaluate 20 RNA transcripts from corneolimbal buttons in a multiplex Luminex-based assay at the indicated times pi according to the manufacturer's instructions. Gene transcripts evaluated are listed in Supplementary Table S1. Real-time PCR was performed as previously described on isolated limbus tissue or isolated PMN to evaluate relative expression of IFNβ, and HSV-1 thymidine kinase (TK) with respect to β-actin.[28] Primer sequences are listed in Table 1.

ELISA and Bioplex Assays

ELISAs were performed on supernatants from corneolimbal buttons homogenized in 1× PBS containing 1× Calbiochem protease inhibitor set 1 (EMD Millipore) at the indicated times pi for IFNα and IFNβ (PBL Assay Science, Piscataway, NJ, USA), TNFα and IL-33 (R&D Systems, Minneapolis, MN, USA), and c-x-c motif chemokine ligand (CXCL) 5 and myeloperoxidase (MPO; Abcam) according to the manufacturer's directions and analyzed with a BMG labtech Fluostar Omega plate reader (Cary, NC, USA). Milliplex Map Luminex-based assays were used to quantify protein levels of c-c motif chemokine ligand (CCL) 2, CXCL1, CXCL2, and CXCL10 in tandem with tissue homogenates used for ELISAs according to the manufacturer's directions. All Luminex-based assays were analyzed on a Bio-Rad Bioplex System (Hercules, CA, USA).

Eicosanoid Analysis

Corneolimbal buttons were obtained at indicated times pi and subsequently analyzed for eicosanoid metabolites by the Lipid MAPS Consortium lipidomics service core at the University of California San Diego via liquid chromatography-tandem mass spectrometry (LC-MS/MS). Sample analysis was performed on a fee-for-service basis. Eicosanoid metabolites analyzed are listed in Table 2. For more information, visit the website http://www.ucsd-lipidmaps.org/ (in the public domain).

Adoptive Transfer

$Ly6G^+$ cells were immunomagnetically isolated as described above from pooled corneas of infected WT mice at 48 hours pi. The number of isolated cells was calculated with a Bio-Rad TC-10 automatic cell counter. Via retroorbital injection, 2×10^5

Table 2. Lipidomic Analysis of Corneal Eicosanoid Metabolites Following HSV-1 Infection

	Uninfected		24 h pi		48 h pi	
Analyte	**WT**	**Kit$^{W\text{-}sh}$**	**WT**	**Kit$^{W\text{-}sh}$**	**WT**	**Kit$^{W\text{-}sh}$**
AA	6.793 ± 1.015	6.215 ± 0.586	4.751 ± 0.934	7.199 ± 1.307	5.093 ± 0.632	6.580 ± 1.197
12-HETE	0.475 ± 0.115	0.753 ± 0.157	0.269 ± 0.070	0.307 ± 0.036	0.579 ± 0.070	0.545 ± 0.091
HXB3	0.1373 ± 0.063	0.117 ± 0.022	0.075 ± 0.037	0.026 ± 0.007	0.122 ± 0.026	0.077 ± 0.027
LTB4	0.003 ± 0.001	0.004 ± 0.001	0.003 ± 0.001	0.001 ± <0.001	0.003 ± 0.001	0.003 ± <0.001
PGD2	0.430 ± 0.089	0.222 ± 0.017	0.354 ± 0.106	0.233 ± 0.050	0.353 ± 0.061	0.330 ± 0.020
PGE2	0.456 ± 0.122	0.341 ± 0.396	0.552 ± 0.178	0.347 ± 0.326	0.503 ± 0.084	0.467 ± 0.067

Not detected: RVD1, RVE1, PD1, 17-HDoHE, HXA3, 7-MaR1. Data reflect nanomoles analyte per milligram corneolimbal button ± SEM ($n = 3$ uninfected, 5–6 infected corneolimbal button pairs per group; 2–3 independent experiments).

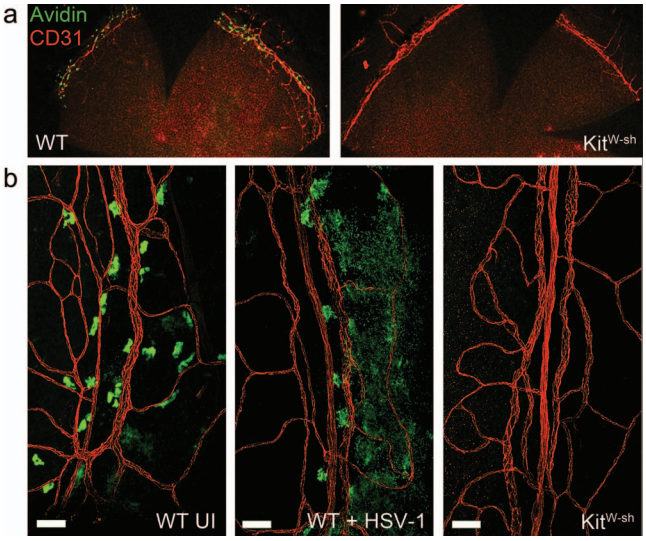

FIGURE 1. Mast cells surround the cornea in the limbus and respond to corneal HSV-1 infection. (**a**) Corneolimbal button whole-mounts from WT and Kit$^{W\text{-}sh}$ mice show MCs (*green*) near the CD31$^+$ limbal vasculature (*red*). (**b**) Limbus-associated MC from uninfected (UI) WT mice have smooth, regular edges (*left*). Limbus-associated MC from WT mice at 24 hours pi with 1000 PFU HSV-1 per eye have a degranulated phenotype (*center*), and are absent in the tissue from Kit$^{W\text{-}sh}$ mice (*right*). *Scale bar*: 50 μm. Images are representative of two independent experiments (n = 2–3 corneas per group). Representative images of limbus-associated MC were acquired using an Olympus MVX-10 epifluorescent microscope with ×16 zoom (**a**) or Olympus FV-500 confocal microscope with a ×20 objective (**b**).

isolated cells were adoptively transferred into CD118$^{-/-}$ mice. Survival was evaluated through day 30 pi.

Leukocyte Histology

Slides were prepared from immunomagnetically isolated Ly6G$^+$ cells isolated from the corneas or spleens of infected mice using a Wescor Cytopro 7620 cytocentrifuge using the manufacturer's suggested settings (Logan, UT, USA). Cytospin preparations were allowed to air dry for 1 hour and then stained using Dade Behring's Diff-Quik stain set according to the manufacturer's instructions (Deerfield, IL, USA). Diff-Quik was also used to stain blood smears prepared from peripheral blood.

In Vitro PMN Infection

Immunomagnetically isolated Ly6G$^+$ cells (PMNs) from pooled peripheral blood were cultured in 24 well plates containing 25,000 cells/well in 1.0 mL normal media and infected with HSV-1 at 0.5 MOI (12,000 PFU). Whole blood was processed as described above via addition of EDTA and red cell lysis buffer prior to immunomagnetic isolation. Neutrophils or HSV-1–only control cultures were collected 18 hours pi, subjected to three freeze/thaw cycles at –80°C/4°C, and supernatants were titered for standard plaque assay.

In Vitro T-Cell Functional Assays

Single cell suspensions of splenocytes were prepared as described above, and counted using a Bio-Rad TC-10 automated cell counter. For functional assays, 1×10^6 splenocytes were cultured in 1.0 mL normal media for 3 hours at 37°C, 5.0% CO_2 in the presence of DMSO as a vehicle control, 2.0 μg $gB_{498\text{-}505}$ peptide, or 50.0 ng PMA and 800 ng ionomycin. After 1 hour in culture, 0.67 μL GolgiStop protein transport inhibitor solution/

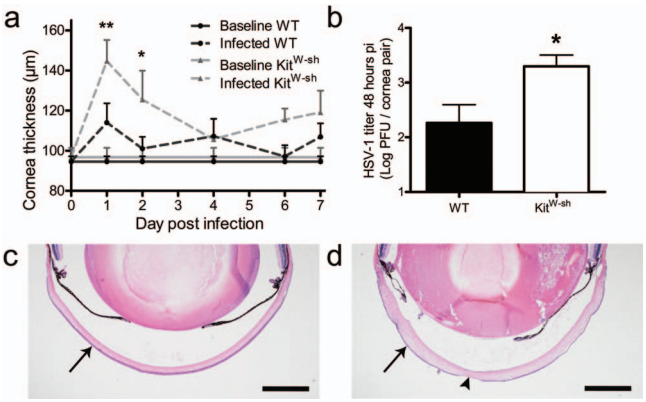

FIGURE 2. Mast cell deficiency leads to increased corneal edema and viral titer. (**a**) Pachymetry was used to measure cornea thickness at the indicated times pi in WT and Kit$^{W\text{-}sh}$ mice following infection with 1000 PFU HSV-1/eye (n = 9–18 corneas per group). The *bars* reflect mean ± SEM of three to four independent experiments per time point. (**b**) Viral loads were measured in corneas of WT and Kit$^{W\text{-}sh}$ mice at 48 hours pi by plaque assay. *Bars* represent mean log PFU/cornea pair ± SEM (n = 6 mice per group) for three independent experiments. Hematoxylin and eosin–stained eye sections illustrating the layered cornea (*arrows*) in UI WT (**c**) and infected edematous Kit$^{W\text{-}sh}$ corneas at day 7 pi (**d**). *Arrowhead* in ([**d**], *bottom center*) shows HSV-1–induced lesion in the corneal epithelium. *Scale bar*: 500 μm. Images were acquired with an Olympus MVX-10 microscope with ×16 zoom and are representative to illustrate data gathered by corneal pachymetry in (**a**).

Monensin (BD Biosciences) was added to facilitate intracellular IFNγ labeling.

Statistical Analysis

Normal distribution was assumed a priori for all data sets. All data is graphed as mean ± SEM and statistical analyses were performed using GraphPad Prism 5 (La Jolla, CA, USA). Student's t-tests were used to determine significant differences ($^*P < 0.05$, $^{**}P < 0.01$, $^{***}P < 0.001$) between groups. A one-way ANOVA was used to analyze plaque assay data for the in vitro PMN infection experiments; a two-way ANOVA was used to analyze data from the pachymetry time course. Tukey's correction for multiple comparisons and multiplicity adjusted P values for each comparison ($^*P < 0.05$, $^{**}P < 0.01$, $^{***}P < 0.001$) were used to identify specific statistical differences between groups identified by ANOVA.

Results

Limbus-Associated MCs Respond to HSV-1 Infection in the Cornea

In humans, MCs are present in the vascularized limbus surrounding the cornea but absent from the cornea proper. To the best of our knowledge, limbus-associated MCs have not previously been described in mice. Mast cells surround the cornea in close association with CD31$^+$ blood vessels in the limbus of WT, but not MC-deficient Kit$^{W\text{-}sh}$ mice via avidin staining of MC granules in fixed corneolimbal button whole-mounts (Fig. 1). These MCs degranulate in response to corneal HSV-1 infection in WT mice (Fig. 1b). Mast cell degranulation was also evaluated in corneas following partial epithelial debridement without the addition of virus, but degranulation was only observed regionally or sporadically after 24 hours in this control group (data not shown).

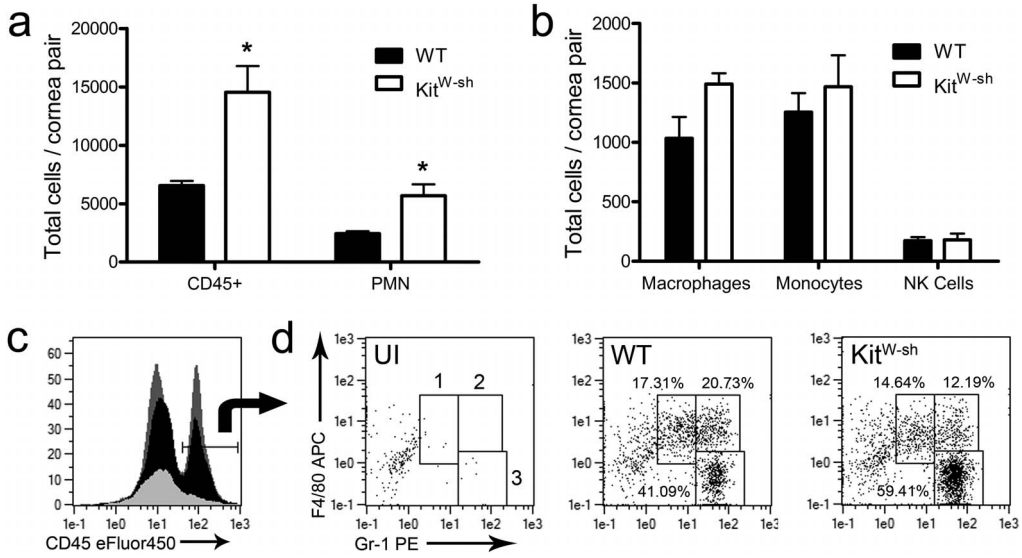

Figure 3. Neutrophil influx is increased in the absence of mast cells. Twenty-four hours pi, cornea pairs from WT and Kit$^{W\text{-}sh}$ mice were harvested and digested in type I collagenase. Single cell suspensions were labeled with antigen-specific monoclonal antibodies and gated to identify CD45^{hi} total leukocytes (**a**, **b**); F4/80^{-} Gr-1^{+} PMN (**a**, **d3**); F4/80^{+} Gr-1^{-} macrophages (**b**, **d1**); F4/80^{+} Gr-1^{+} inflammatory monocytes (**b**, **d2**); and CD3^{-} NK1.1^{+} NK cells by flow cytometry. Representative histograms for CD45 expression (overlay: *dark gray* = Kit$^{W\text{-}sh}$ 24 hours pi, *black* = WT 24 hours pi, *light gray* = UI WT) and *dot plots* for F4/80 and Gr-1 expression are presented in (**c**) and (**d**), respectively. Relative frequencies of these populations are shown in the *dot plots*. Data reflect two independent experiments ($n = 5$ mice/group) and is shown as mean ± SEM.

Degranulation is the initial MC response to activation and is followed by de novo synthesis of many products. To investigate whether MCs modulate the host innate response to HSV-1 beyond degranulation, a luminex-based RNA array was used to analyze 18 gene transcripts noted for MC-modulatory effects or known to be MC products (Supplementary Table S1) at 24 and 48 hours pi in corneolimbal buttons from WT and Kit$^{W\text{-}sh}$ mice. Excessive variability limited the usefulness of this assay. However, trends in higher expression of IFNα4, IFNγ, and IL-1β transcripts were noted in WT samples at 48 hours pi (Supplementary Fig. S1). To further evaluate whether limbus-associated MCs may directly contribute to the production of type I IFNs, IFNβ expression was separately measured by real-time PCR in isolated limbus tissue of WT and Kit$^{W\text{-}sh}$ mice at 48 hours pi; however, no difference was observed (data not shown). Tumor necrosis factor-α enhances leukocyte recruitment to infected tissues, but also mediates direct antiviral effects on HSV-1.[29] No difference in TNFα transcript expression was observed in the RNA array (data not shown) comparing WT and Kit$^{W\text{-}sh}$ corneas. Protein levels of IFNα, IFNβ, and TNFα were analyzed by ELISA in corneolimbal buttons, but the expression was below the limit of detection at 18 to 24 hours pi.

MC Deficiency Leads to Increased Corneal Edema and Viral Titer

Tissue edema is often associated with the proinflammatory activities of MCs. Cornea thickness was monitored over the course of acute HSV-1 infection in WT and Kit$^{W\text{-}sh}$ mice by pachymetry (Fig. 2a). Cornea thickness did not differ between healthy WT and Kit$^{W\text{-}sh}$ mice. Surprisingly, corneas of Kit$^{W\text{-}sh}$ mice were significantly more edematous throughout the first 48 hours pi compared with WT. Cornea thickness remained elevated above baseline in Kit$^{W\text{-}sh}$ mice throughout most of the observation period. Corneal HSV-1 titers were no different comparing WT and Kit$^{W\text{-}sh}$ mice at 20 hours pi, a time point consistent with one round of viral replication (data not shown). However, Kit$^{W\text{-}sh}$ mice had significantly higher HSV-1 titers in

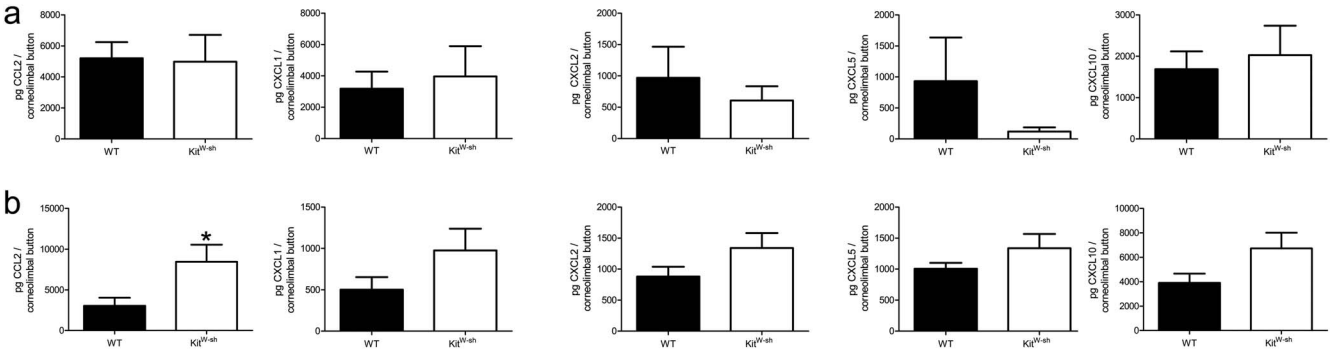

Figure 4. Cytokine production in corneolimbal buttons of WT and Kit$^{W\text{-}sh}$ mice. Corneolimbal buttons were harvested at 18 (**a**) and 48 (**b**) hours pi, homogenized in 1× PBS containing 1× protease inhibitor cocktail, and supernatant was used for analysis of picogram (pg) protein per corneolimbal button. Results reflect six corneolimbal buttons per group (two independent experiments) shown as mean ± SEM.

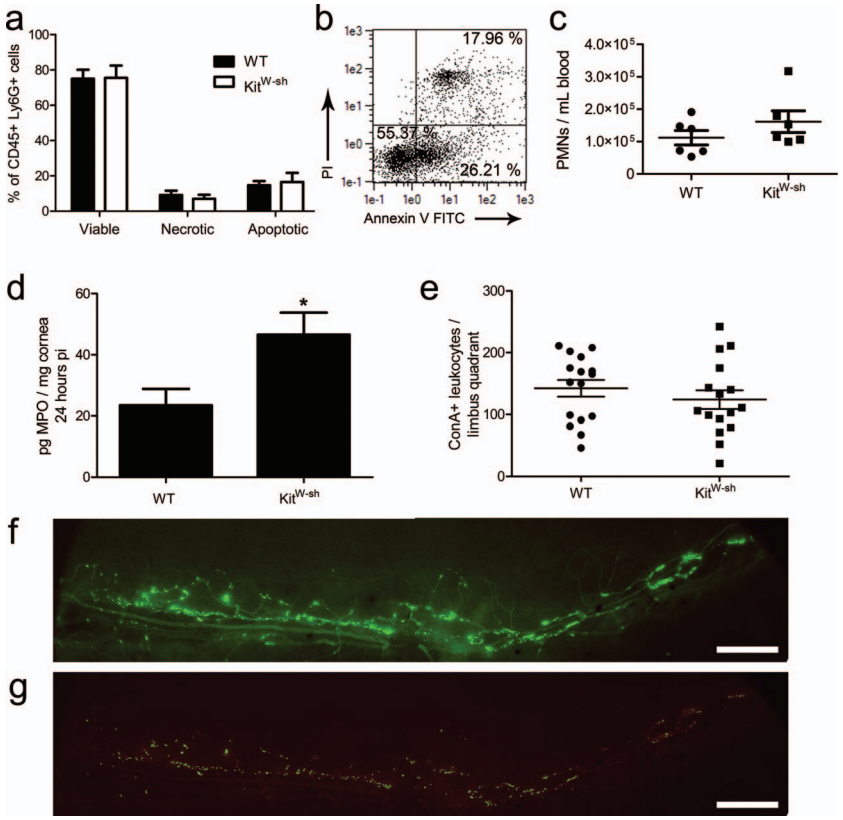

Figure 5. Neutrophil characteristics and leukostasis in the limbus. Corneas were harvested from WT and Kit$^{W\text{-}sh}$ mice at 24 hours pi, digested in type 1 collagenase, immunolabeled, and analyzed by flow cytometry for CD45$^+$ Ly6G$^+$ PMN with propidium iodide (PI) and annexin V staining for viability analysis (**a**). Results reflect % total PMN in five mice per group (two independent experiments). (**b**) Representative dot plot from a WT mouse showing PI and annexin V analysis: LLQ (PI$^-$ annexin V$^-$) = viable; LRQ (PI$^-$ annexin V$^+$) = apoptotic; URQ (PI$^+$ annexin V$^+$) = necrotic. (**c**) Neutrophils counts in peripheral blood at 48 hours pi ($n = 6$ mice per group; three independent experiments) evaluated by flow cytometric analysis as shown in Figure 3. (**d**) Total MPO was evaluated by ELISA at 24 hours pi ($n = 9$ samples/group; three independent experiments). Myeloperoxidase production was not detected in uninfected corneas of WT and Kit$^{W\text{-}sh}$ mice (not shown). Total leukocytes adhering to the limbal vasculature in pericorneal quadrants 24 hours pi (**e**) visualized by ConA perfusion staining. Results show total leukocytes/quadrant representing 16 limbus quadrants from four corneas per group (three independent experiments). All data graphed as mean ± SEM. (**f**) Epifluorescent micrograph depicting ConA staining of vasculature (*dim*) and leukocytes (*bright*) in a limbal quadrant used for analysis in (**e**). (**g**) Color-intensity adjusted rendering of limbus in (**f**) to eliminate ConA+ vasculature for quantification of adherent ConA bright leukocytes. Images were obtained using an Olympus MVX-10 epifluorescent microscope at ×1.6 magnification (*scale bar*: 200 μm).

the cornea at 48 hours pi (Fig. 2b). Corneal edema can be appreciated in hematoxylin and eosin (H&E)-stained sections comparing an uninfected (UI) eye to an infected Kit$^{W\text{-}sh}$ eye at day 7 pi in Figures 2c and 2d, respectively. By day 7 pi, virus-mediated lesions are present in the corneal epithelium and edema is most apparent in the stroma (Fig. 2d).

To further examine the impact of preformed MC mediators on corneal HSV-1 infection, we assessed corneal viral titers at 48 hours pi in WT and Kit$^{W\text{-}sh}$ mice treated with supplemental histamine at the time of infection. No difference in corneal HSV-1 titer was observed in WT mice treated topically with 1 μM or 100 μM histamine in a 3-μL eyedrop at the time of infection compared with vehicle control-treated mice (Supplementary Fig. S2a). However, application of histamine to the corneas of Kit$^{W\text{-}sh}$ mice in separate experiments revealed a nonsignificant trend toward a dose-dependent increase in viral titer for the concentrations evaluated relative to their vehicle control-treated counterparts (Supplementary Fig. S2b). Histamine concentrations were based on dose-response curves of human corneal epithelial cell cytokine production following histamine stimulation in vitro.[30] Herpes simplex virus type-1 titer was also assessed by comparing WT and TNFα-deficient mice at 48 hours pi, but no difference was observed (Supplementary Fig. S2c).

Neutrophil Influx Is Increased in the Absence of MCs

Flow cytometry was used to analyze leukocyte influx into corneas from WT and Kit$^{W\text{-}sh}$ mice at 24 hours pi. Corneas from Kit$^{W\text{-}sh}$ mice had significantly more total CD45$^+$ leukocytes with an increase in the F4/80$^-$ Gr-1$^+$ PMN population (Figs. 3a, 3c, 3d). While there was a nonsignificant rise in the F4/80$^+$ Gr-1$^-$ macrophage population present, no differences were observed in the numbers of F4/80$^+$ Gr-1$^+$ inflammatory monocytes (Figs. 3b, 3d) or CD3$^-$ NK1.1$^+$ NK cells (data not shown). No difference was observed in NK cell activation receptor NKG2D expression by mean fluorescence intensity (MFI) between the two groups (data not shown).

Soluble factors including cytokines, chemokines, and type-1 IFNs coordinate leukocyte influx and promote antiviral responses during corneal HSV-1 infection. Protein levels of chemokines responsible for PMN chemotaxis including CXCL1, CXCL2, and CXCL5 were measured at 18 and 48 hours pi in corneolimbal buttons of WT and Kit$^{W\text{-}sh}$ mice. CCL2, and CXCL10 were also analyzed due to their respective correlations with either HSV-1 titer or inflammation and PMN influx in the cornea.[8,31] By 18 hours pi, there were no

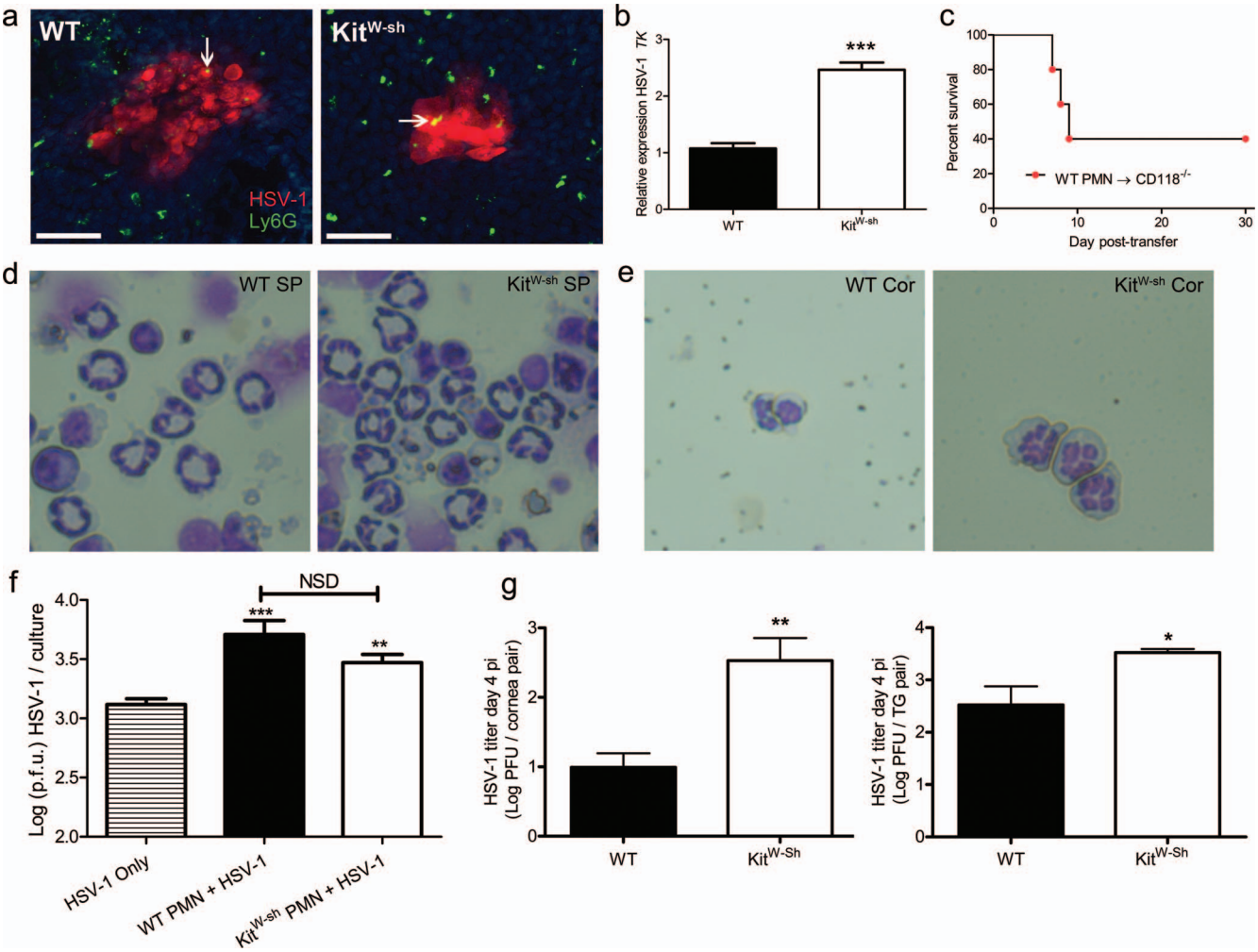

Figure 6. Neutrophils facilitate HSV-1 replication through viral hijacking. (**a**) Confocal microscopy was used to visualize DAPI-stained nuclei (*blue*), HSV-1 antigen (*red*), and Ly6G$^+$ PMN (*green*) in WT and Kit$^{W\text{-}sh}$ cornea whole-mounts at 48 hours pi. Representative images of five corneas per group are shown (two to three independent experiments). Images were obtained using an Olympus FV-500 confocal microscope with a ×20 objective; images reflect additional ×3 digital zoom. *Scale bar*: 50 μm. *Arrows* point to regions of PMN and HSV-1 colocalization. (**b**) Real-time PCR analysis of HSV-1 *TK* relative to β-actin in Ly6G$^+$ neutrophils immunomagnetically enriched from pooled WT or Kit$^{W\text{-}sh}$ corneas harvested at 48 hours pi and digested in type I collagenase. Expression normalized to WT PMN. *TK* was detected in both WT- and Kit$^{W\text{-}sh}$-derived PMN. Data reflect two to four RT-PCR reactions on 2×10^4 PMN isolated from pooled infected corneas of 6 to 10 mice per group (two independent experiments). (**c**) Survival of CD118$^{-/-}$ mice following intravenous adoptive transfer of 2×10^4 PMN isolated from pooled WT corneas (12 mice) as in (**b**) delivered via retro-orbital injection ($n = 6$ CD118$^{-/-}$ mice; two independent experiments). Data reported as a percentage of survival of CD118$^{-/-}$ mice through day 30 post transfer. Each data point represents one CD118$^{-/-}$ mouse. Representative images shown in (**d**) and (**e**) are cytospin preparations of Diff-Quik stained Ly6G$^+$ cells recovered from spleens (**d**) showing ring-shaped nuclear morphology and infected corneas (**e**) showing segmented nuclei at 48 hours pi (×96 magnification). (**f**) Ly6G$^+$ cells (PMNs) isolated from peripheral blood were infected at 0.5 MOI with HSV-1 and evaluated for viral titer 18 hours pi to show that PMNs are sufficient for HSV-1 replication ($n = 8$–12 cultures containing 25,000 PMNs per culture; two independent experiments). A one-way ANOVA with Tukey's correction for multiple comparisons was used to calculate statistical differences in HSV-1 titers in infected PMN cultures over HSV-1 only control cultures. (**g**) Herpes simplex virus type-1 titer in the corneas and TG of WT and Kit$^{W\text{-}sh}$ mice at day 4 pi ($n = 5$ animals/group; two independent experiments).

differences in the amount of any chemokines analyzed between WT and Kit$^{W\text{-}sh}$ mice (Fig. 4a). However, a trend in elevated levels of CXCL1, CXCL2, CXCL5, and CXCL10 proteins in Kit$^{W\text{-}sh}$ mice were observed at 48 hours pi (Fig. 4b). Macrophage/monocyte-derived CCL2 was significantly elevated in Kit$^{W\text{-}sh}$ mice (Fig. 4b).

Danger-induced inflammation can also promote PMN influx through IL-33 upregulation, and IL-33 is reportedly modulated by MC-mediated degradation via MC-protease 4 (MCPT-4).[32–34] ELISA results confirmed that IL-33 is constitutively expressed in the cornea. No difference in total IL-33 expression was detected between infected corneas of WT or Kit$^{W\text{-}sh}$ mice at 24 hours pi despite the approximate 2-fold increase in IL-33 expression following HSV-1 infection (data not shown).

Neutrophil Characteristics and Leukostasis in the Limbus

Mast cells boost PMN effector function in response to lipopolysaccharide (LPS)-induced lung inflammation in vivo and delay PMN apoptosis in vitro.[35] Neutrophil viability was assessed by flow cytometry in cells isolated from infected corneas of WT and Kit$^{W\text{-}sh}$ mice at 24 hours pi. There were no differences in the percentage of viable, apoptotic, or necrotic

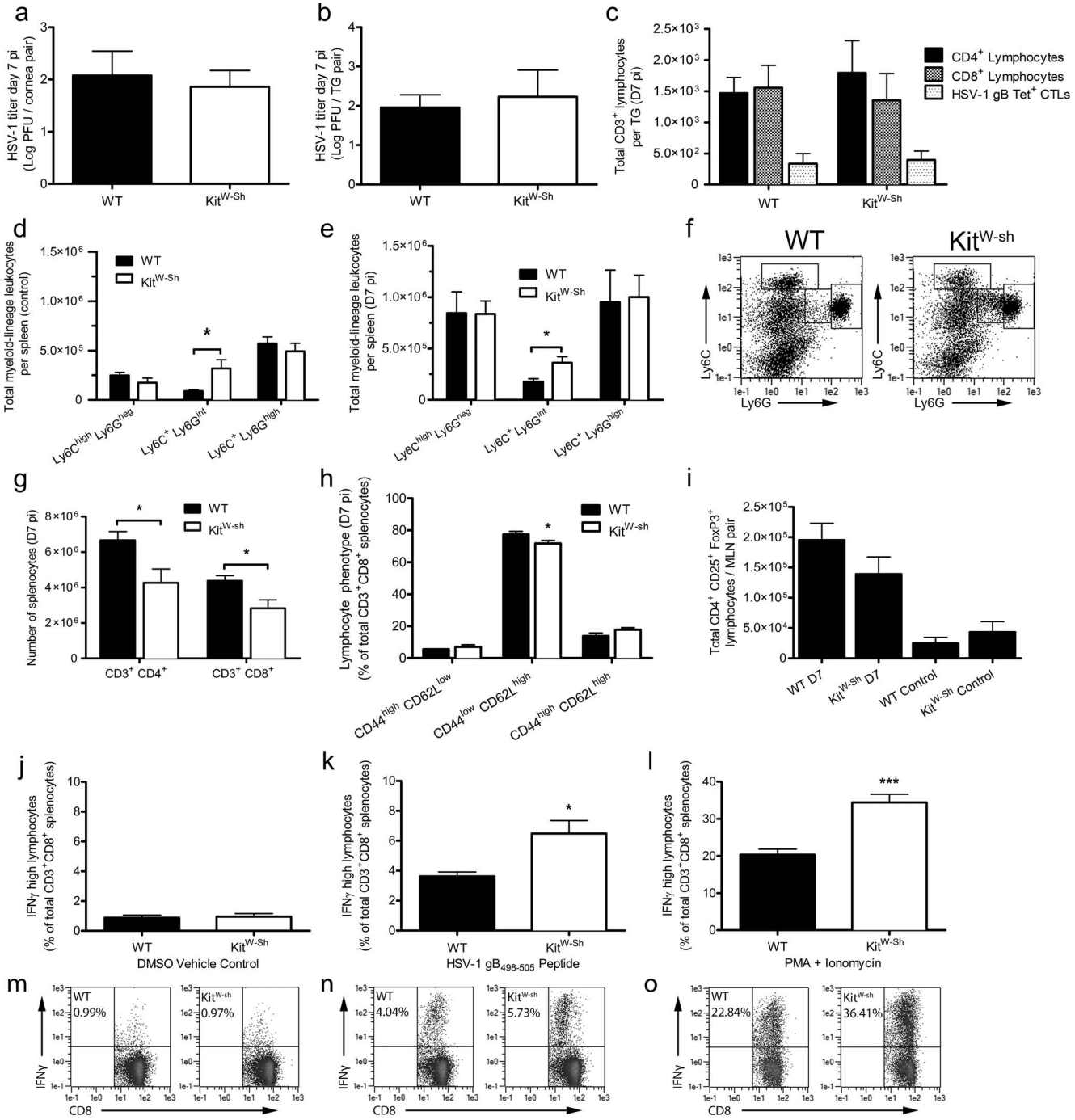

Figure 7. Myeloid-derived suppressor cells have no impact on local innate or systemic adaptive immune responses to acute HSV-1 infection. Viral loads were measured in corneas (**a**) and TG (**b**) of WT and Kit$^{W\text{-}sh}$ mice at D7 pi by plaque assay. *Bars* represent mean log PFU/cornea pair ($n = 8$ mice/group; three independent experiments) or log PFU/TG pair ($n = 6$ mice/group; three independent experiments). (**c**) T-cell infiltration in the TG at D7 pi. *Bars* reflect the total number of CD4$^+$, CD8$^+$, and HSV-specific CD8$^+$ cytotoxic T cells (CD3$^+$) by tetramer labeling for the immunodominant epitope of HSV-1, gB$_{498\text{-}505}$ (gB Tet$^+$ CTLs) per TG pair ($n = 7$–10 mice/group; three independent experiments). Distribution of CD45$^+$ CD11b$^+$ splenocyte populations in control mice at 0 to 18 hours pi (**d**) and mice at D7 pi (**e**) based on differential Ly6C and Ly6G expression ($n = 4$ mice/control group and 7 mice/group at D7pi; three independent experiments). Representative dot plots from control mice highlight the three populations analyzed (**f**). The total number of CD3$^+$ CD4$^+$/CD8$^+$ T-cell in spleens of WT and Kit$^{W\text{-}sh}$ mice at D7 pi are shown in (**G**) ($n = 10$ mice/group; four independent experiments). Splenic CD3$^+$ CD8$^+$ T-cell phenotype was evaluated based on CD44 and CD62L expression (**h**) at D7 pi ($n = 6$ mice/group; three independent experiments). (**i**) Total CD4$^+$ CD25$^+$ FoxP3$^+$ Tregs in the mandibular lymph nodes at indicated times pi (control reflects 0–18 hours pi; $n = 4$–5 mice/control group and 8 mice/group at D7 pi; two to three independent experiments). Interferon-γ production in CD3$^+$ CD8$^+$ T cells cultured from total splenocytes harvested at D7 pi in vitro following stimulation with DMSO (**j**), HSV-1 gB$_{498\text{-}505}$ peptide (**k**), and PMA + ionomycin (**l**). Data reflect the frequency of IFNγ^{high} CD8$^+$ T cells ($n = 5$ mice/group; three independent experiments). Representative *dot plots* for each group are shown below in (**m**), (**n**), and (**o**), respectively. All data reflect mean ± SEM.

CD45$^+$ Ly6G$^+$ PMNs by propidium iodide and annexin V staining (Figs. 5a, 5b). Moreover, the increase in cornea-infiltrating PMNs correlated with a proportionate elevation of MPO in corneas from Kit$^{W\text{-}sh}$ mice relative to WT by ELISA, pointing to no functional deficiency in the Kit$^{W\text{-}sh}$ PMNs responding to infection (Fig. 5d). Neutrophilia and splenomegaly have also been reported in Kit$^{W\text{-}sh}$ mice.[36] In our model, there was no significant difference in the number of circulating PMN/mL of peripheral blood at 48 hours pi comparing WT and Kit$^{W\text{-}sh}$ mice; only one of six Kit$^{W\text{-}sh}$ mice surveyed exhibited neutrophilia (Fig. 5c). Furthermore, gross splenomegaly was seldom observed in Kit$^{W\text{-}sh}$ mice housed in our specific pathogen-free animal facility (~1 in 15–20 mice; data not shown).

Another possible means to explain the increase in PMNs in the cornea in the early response to local HSV-1 infection is due to nonspecific leukostasis. Therefore, the number of leukocytes adhering to the limbal vasculature proximal to the cornea at 24 hours pi was analyzed by concanavalin A (ConA) lectin perfusion. We found no cumulative difference in the number of limbus-adherent leukocytes between WT and Kit$^{W\text{-}sh}$ mice (Fig. 5e). Representative images of the ConA-labeled limbal vasculature and leukocytes in addition to an intensity-adjusted rendering of the image used to quantify leukocytes are shown in Figures 5f and 5g, respectively.

The Corneal Eicosanoid Profile Following HSV-1 Infection Is Largely MC-Independent

Cytokines and chemokines are the hallmark mediators of inflammation, but the lipid counterparts of these proteins, the eicosanoids, also modulate inflammation and its resolution through direct chemotaxis of leukocytes and regulation of vascular permeability. The profile of uninfected and infected corneolimbal buttons from WT and Kit$^{W\text{-}sh}$ mice were analyzed in a modest lipidomics screen in order to evaluate the impact of eicosanoids on corneal inflammation and PMN infiltration during the first 48 hours pi. Resolvin D1 (RVD1), resolvin E1 (RVE1), protectin D1 (PD1), 17-hydroxy docsahexaenoid acid (17-HDoHE; the PD1 precursor), 7(R) maresin-1 (7-MaR1), and hepoxilin A3 (HXA3) were not detected in uninfected or infected tissue in the presence or absence of MCs. Nanomole quantities per tissue mass of prostaglandin E2 (PGE2), prostaglandin D2 (PGD2), leukotriene B4 (LTB4), 12-hydroxyeicosatetraenoic acid (12-HETE), hypoxilin B3 (HXB3), and total arachidonic acid (AA) are recorded in Table 2. The profiles of detected analytes in infected tissue were unremarkable. However, an approximate 50% reduction of PGD2 and 30% increase of 12-HETE were observed in uninfected corneolimbal buttons from Kit$^{W\text{-}sh}$ mice relative to WT.

Neutrophils Facilitate HSV-1 Replication and Dissemination

Confocal microscopy was utilized to image PMNs and HSV-1 infected cells in the central corneas of WT and Kit$^{W\text{-}sh}$ mice. Both groups displayed HSV-1 antigen in corneal lesions. Neutrophils were found throughout the corneas of WT and Kit$^{W\text{-}sh}$ mice. Some PMNs colocalized with HSV-1 antigen in corneal lesions (Fig. 6a). Neutrophils were subsequently isolated from pooled corneas of WT or Kit$^{W\text{-}sh}$ mice at 48 hours pi by Ly6G$^+$ immunomagnetic isolation. Isolated PMNs were greater than or equal to 90% pure by flow cytometric analysis using CD11b$^+$ Gr-1$^+$ colabeling for identification. The HSV-1 lytic gene encoding *TK* was expressed in Ly6G$^+$ cells isolated from both WT and Kit$^{W\text{-}sh}$ corneas, but not in circulating PMN obtained from uninfected mice. Moreover, the level of *TK* expression was more than 2-fold higher in PMN isolated from Kit$^{W\text{-}sh}$ mice (Fig. 6b).

Owing to the significance of HSV-1 replication in PMN, we found the majority of viral sentinel type I IFN receptor deficient (CD118$^{-/-}$) mice succumbed to infection following adoptive transfer of Ly6G$^+$ cells isolated from corneas of infected WT mice (Fig. 6c). Ly6G$^+$ cells isolated from peripheral blood of uninfected WT and Kit$^{W\text{-}sh}$ mice and incubated with HSV-1 in vitro facilitated viral replication, as assessed by plaque assay (Fig. 6f). Unbridled PMN infiltration into HSV-1 infected corneas in vivo contributes to local viral replication and enhances dissemination to the peripheral nervous system, as HSV-1 titers in the corneas and TG were significantly higher in Kit$^{W\text{-}sh}$ mice compared to WT at day 4 pi (Fig. 6g).

MDSC Do Not Alter the Innate or Adaptive Immune Response to Acute HSV-1 Infection

Myeloid-derived suppressor cells have been described in chronic disease states and are noted for their ability to potently suppress T-cell responses.[37] Myeloid-derived suppressor cells are a heterogeneous population of granulocytic and monocytic (G/M-MDSC) populations.[37] Michel et al.[38] have described an enriched population of Gr-1$^+$ cells in the spleen of Kit$^{W\text{-}sh}$ mice exhibiting ring-shaped nuclei consistent with MDSC. To evaluate the impact of MDSC in our HSV-1 infection model using Kit$^{W\text{-}sh}$ mice, we investigated the presence of MDSC in the cornea at 48 hours pi and their functional impact on early adaptive immune response to HSV-1 at day 7 (D7) pi in the spleen.

The nuclear morphology of Ly6G$^+$ cells recovered from the cornea and spleen of WT and Kit$^{W\text{-}sh}$ mice were compared by modified Wright Giemsa-stained cytospin preparations at 48 hours pi (Figs. 6d, 6e). The majority of Ly6G$^+$ cells recovered from the spleen of both strains showed distinctive ring-shaped nuclei with open centers larger than the cross-sectional diameter of the ring (Fig. 6d). In contrast, the nuclear morphology of Ly6G$^+$ cells recovered from corneas exhibited lobe-like patterning consistent with PMNs and not MDSC (Fig. 6e). Leukocytes with ring-shaped nuclei consistent with MDSC or band cells were observed in the peripheral blood smears of both genotypes, but these cells were rare (data not shown).

The adaptive immune response begins to control HSV-1 infection by D7 pi. Consistent with the induction of an adaptive immune response, HSV-1 titers did not differ between WT and Kit$^{W\text{-}sh}$ mice at D7 pi in the corneas or TG (Figs. 7a, 7b). Flow cytometry was used to evaluate T-cell infiltration in the TG of infected WT and Kit$^{W\text{-}sh}$ mice at D7 pi. No differences in the number of CD4$^+$ or CD8$^+$ T cells were observed between the two groups. Moreover, there was no difference in the total number of HSV-1-specific CD8$^+$ T cells (Fig. 7c) by MHC-tetramer labeling for the primary immunodominant epitope of HSV-1 in C57BL/6J mice, glycoprotein B ($gB_{498\text{-}505}$).

To better understand how myeloid-lineage cells affect the T-cell response during acute HSV-1 infection, we tracked the expansion and phenotype of various populations of CD11b$^+$ myeloid cells based on differential expression of Ly6C and Ly6G (Figs. 7d, 7e) as well as the number of CD4$^+$ and CD8$^+$ T cells (Fig. 7g) in the spleen by flow cytometry. By D7 pi, the Ly6C^{high} Ly6G^{neg} and Ly6C$^+$ Ly6G^{high} populations expanded 2- to 3-fold over controls (0–18 hours pi) in both WT and Kit$^{W\text{-}sh}$ mice; conversely, the Ly6C$^+$ Ly6G^{int} population described by Michel et al.[38] as M-MDSC did not expand from baseline levels by D7 pi in either genotype (Figs. 7d–f). There were fewer CD4$^+$ and CD8$^+$ T cells in the spleens of Kit$^{W\text{-}sh}$ mice at D7 pi (Fig. 7g). However, this difference could only account for a

reduction of $CD44^{low}$ $CD62L^{high}$ naive T cells in $Kit^{W\text{-}sh}$ mice (Fig. 7h). No differences were detected in the frequency of $CD44^{high}$ $CD62L^{high/low}$ central/effector memory $CD8^+$ T cells, respectively (Fig. 7h).

We also evaluated the total number of $CD4^+$ $CD25^+$ $FoxP3^+$ regulatory T cells (Treg) in the mandibular lymph nodes of naive and infected $Kit^{W\text{-}sh}$ and WT mice at D7 pi. Treg expansion was observed, but we found no statistically significant differences in the total number of Tregs at either timepoint (Fig. 7i).

Because MDSC are capable of suppressing antigen specific and nonspecific T-cell function,[37] we evaluated the impact of the myeloid cell distribution in WT and $Kit^{W\text{-}sh}$ spleens at D7 pi relative to $CD8^+$ T-cell responsiveness in vitro. Negligible IFNγ production by $CD8^+$ T cells was observed when splenocytes were cultured in media containing DMSO as a vehicle-control (Fig. 7j). However, by adding recombinant $gB_{498\text{-}505}$ peptide or PMA and ionomycin to the cultures, we observed a significant increase in the frequency of $IFN\gamma^{high}$ $CD8^+$ T cells from $Kit^{W\text{-}sh}$ mice over WT animals (Figs. 7k, 7l).

Discussion

The function of MCs has been rather elusive to immunologists since Paul Ehrlich discovered them in the late 19th century. Mast cells are best characterized for their role in mediating allergic responses, but MCs are also important for pathogen surveillance and defense in mucosal tissues.[18] Mast cells were identified in the human limbus five decades ago by transmission electron microscopy, but have been largely overlooked with respect to pathologies in the anterior eye aside from allergy.[25]

Efficient pathogen detection and clearance as well as maintenance of the corneal tissue architecture are critical for the preservation of visual acuity. Mast cells are pleiotropic leukocytes and represent a double-edged sword for inflammation in the anterior eye. Mast cells drive inflammation in ocular allergy. However, our data demonstrate MCs limit inflammation and antagonize virus replication most likely by regulating the influx of PMNs that, in turn, act as a reservoir for additional viral replication. This is consistent with a loss of fidelity in the innate immune response in the absence of MCs, such that corneal viral replication and neurotropic spread of HSV-1 are enhanced in $Kit^{W\text{-}sh}$ mice.

Though a genetic MC deficiency in humans is not known to exist, we have modeled an ocular infection in MC-deficient $Kit^{W\text{-}sh}$ mice to determine the impact MCs have on the early innate immune response in this mucosal site. The role of MCs in surveillance and defense against HSV-1 and other pathogens in the cornea is particularly relevant clinically due to the array of MC-targeted drugs including corticosteroids, degranulation-inhibiting compounds, and antihistamines routinely used to treat ocular allergy symptoms.[39] In light of our findings, the topical use of MC-targeted drugs for ocular allergy may need to be reconsidered in patients with a history of recurrent HSV-1 reactivation in the cornea.

In our study, corneal HSV-1 titer was not affected by exogenous histamine in WT mice, but this treatment augmented titers in $Kit^{W\text{-}sh}$ mice (Supplementary Fig. S2). While it is clear that MCs are more than a source of histamine, the mechanism underlying the increase in viral titer in response to histamine in $Kit^{W\text{-}sh}$ mice is unclear. $Kit^{W\text{-}sh}$ mice have lower basal levels of histamine than WT mice,[40] and may respond to histamine differently. The pharmacologic impact of histamine is a complex and often controversial topic due to variable expression patterns of its four receptors, H_1R-H_4R.[41,42]

Neutrophils are the most abundant leukocyte population that extravasates into the cornea upon HSV-1 infection. Seminal $Gr\text{-}1^+$ cell depletion experiments suggested that PMNs suppress HSV-1 replication[43]; however, the Gr-1 antigen was subsequently identified on other leukocytes.[8,13] A multidimensional analysis including Ly6C or F4/80 antigen labeling is essential to clearly resolve PMNs by flow cytometry. Furthermore, PMN depletion using the more specific anti-Ly6G antibody has no effect on HSV-1 titer in WT mice.[8,14] Data from the present investigation showing that PMN infiltrate is significantly increased in MC-deficient mice during HSV-1 infection indicate that MCs regulate leukocyte influx into the cornea.

The ability of MCs to upregulate local leukocyte adhesion and vessel permeability is well documented.[17,18] Mast cells have also adapted ways to restrict inflammation to reduce tissue pathology,[19,22,34,44] as MCs have been reported to inhibit PMN infiltration during sterile inflammation in other immune privileged sites through a TLR7 ligand–dependent mechanism.[45] This finding is consistent with recent evidence supporting a role for type-1 IFN in suppressing neutrophil recruitment during HSV-1 infection of the skin.[46] While it has been reported that MCs produce type-1 IFN during viral infection,[47] this aspect of MC physiology could not be clearly ascertained in our model.

Neutrophil chemotaxis in our system is likely due, in part, to collective increases in CXCL-1, -2, and -5, in addition to CXCL10 ranging from 40% to 100% in $Kit^{W\text{-}sh}$ mice over WT (Fig. 4b). CCL2 was significantly increased in the corneas of $Kit^{W\text{-}sh}$ mice (Fig. 4b) by 48 hours pi, but CCL2 is not typically considered to be a PMN chemoattractant. Nonetheless, CCL2 has been reported to recruit PMNs during corneal infection.[48,49] Thus, it cannot be ruled out from this investigation that CCL2 may facilitate PMN influx during corneal HSV-1 infection.

Due to the cytolytic nature of HSV-1 infection, it is likely that danger-induced inflammation plays a role in the innate immune response in addition to direct triggering of pathogen-associated molecular pattern (PAMPs). The alarmin IL-33 was also examined due to its role in danger-induced corneal inflammation, PMN chemotaxis, and MC-mediated degradation.[32–34] MC-protease 4 is associated with degradation of a variety of inflammatory mediators including TNF, IL-33, and endogenous damage-associated molecular patterns (DAMPs) to limit tissue inflammation.[34,44] Our data corroborate the reported finding of constitutive IL-33 expression in the cornea and show it is elevated following HSV-1 infection.

Mast cells are capable of secreting a variety of lipid mediators to facilitate their role in fine-tuning local immune responses prior to de novo cytokine and chemokine synthesis.[17,50] The therapeutic benefit of exogenous RVE1 treatment has been demonstrated using multiple corneal infection models with respect to limiting corneal inflammation.[51,52] We have conducted the first reported lipidomic profiling study of the murine cornea following HSV-1 infection. Data from our lipidomics screen show that corneal HSV-1 infection does not elicit detectible endogenous production of PD1, its precursor 17-HDoHE, 7-Mar1, RVD1, or RVE1 within the first 48 hours pi despite their established role in resolving inflammation.[12,53,54]

Corticosteroids and nonsteroidal anti-inflammatory drugs are known to alter the eicosanoid metabolic profile through pharmacologic effects on cyclooxygenase (COX) and lipoxygenase (LO). Counter-regulatory crosstalk occurs between COX-derived prostaglandins and IFN-α/β signaling.[55] Therefore, obtaining a more thorough understanding of the lipidomic profile and cells that contribute to eicosanoid synthesis in the cornea during HSV-1 infection has important clinical and translational implications.

Arachidonic acid–derived metabolites were screened based on their association with PMN infiltration, such as the

hepoxilins, leukotrienes, and prostaglandins.[56–58] Bioavailability of AA remained comparable in all experimental groups; AA is the substrate for which LO and COX enzymes compete. Eicosanoid profiles observed following HSV-1 infection were largely MC-independent (Table 2). This data is consistent with the previous observation that eicosanoid synthesis during ocular HSV-1 infection primarily occurs in the central cornea.[59] Nonetheless, the corneal–scleral rim is an active site of eicosanoid synthesis during homeostasis.[59]

The ratio of COX-derived PGD2 to LO-derived 12-HETE differed inversely between uninfected corneolimbal buttons of WT and $Kit^{W\text{-}sh}$ mice ($P = 0.021$; data not shown). Specifically, WT mice had a high PGD2:12-HETE ratio and $Kit^{W\text{-}sh}$ mice had a low PGD2:12-HETE ratio. Prostaglandin D2 suppresses PMN chemotaxis and endothelial transmigration during acute inflammation.[60,61] Conversely, 12-HETE is a potent PMN chemoattractant that also promotes increased vascular permeability.[62,63] Mast cell–derived PGD2 (the dominant COX-derived metabolite in MCs) restricts vascular permeability,[64,65] thus MCs likely prevent excess inflammation and help maintain immune privilege in the cornea. A MC–dependent eicosanoid imbalance in the limbus may have an early effect on the ability of circulating PMNs to enter the cornea in the hours following HSV-1 infection.

Our data herein builds a new paradigm that PMNs are susceptible to HSV-1 infection and permissive to virus replication. Our lab has previously identified virally infected $CD11b^+$ cells as contributing to HSV-1 spread to the retina through intravitreal trafficking following corneal infection.[66] Therefore, it is not entirely unexpected that PMNs are susceptible to subterfuge and hijacking by HSV-1, in effect turning them into surrogate leukocytes for HSV-1 replication.

A single permissive cell can generate multiple infectious virions. Thus, we speculate HSV-1 usurps PMNs within corneal viral lesions to generate infectious progeny. The observed differences in viral titer comparing corneas of WT and $Kit^{W\text{-}sh}$ mice coincides with a divergent number of PMNs present in the cornea upon cytolytic release of HSV-1 from the site of initial infection: corneal epithelial cells. We interpret this difference in viral titer between 20 and 48 hours pi to suggest that the corneal epithelium is no more susceptible to HSV-1 infection in the absence of MCs, but that MCs coordinate appropriate innate countermeasures to facilitate viral clearance and restrain neuroinvasion by HSV-1.

The use of $Kit^{W\text{-}sh}$ mice for MC-research has been under scrutiny due to reported immunologic abnormalities, largely centered around the altered expression pattern of MDSC.[38] While we cannot account for the extremedullary myelopoiesis observed in BALB/c $Kit^{W\text{-}sh}$ mice by Michel et al.[38] in our C57BL/6J $Kit^{W\text{-}sh}$ mice housed in a specific pathogen free facility, it is critically important to note that BALB/c was chosen over C57BL/6J in their studies because the splenic myeloid hyperplasia was significantly more severe on the BALB/c background.

Myeloid-derived suppressor cells have remained an enigmatic cell population due to the inability of traditional means of cellular phenotyping (i.e., flow cytometry and microscopy) to stringently and unequivocally define this population separately from other myeloid cells expressing combinations of CD11b, Ly6C, Ly6G, and Gr-1. Nuclear morphology has been used to dileneate MDSC from PMNs based on nuclear segmentation patterns, though this approach is not uniformly helpful in determining suppressive activity.[67] Isolated reports of unique phenotypic traits of MDSC exist, but such reports have failed to gain traction or consensus among investigators in the field.[67–69] Myeloid-derived suppressor cells represent a heterogeneous cell population whose subsets and functions have yet to be examined in the context of the early innate response to acute infection in the eye. Therefore, we sought to define the role of MDSC in our system to ensure that the supposed MC-dependent phenomena were not downstream effects of MDSC. Taken together, our data confirm that PMNs and not MDSC are the $Gr\text{-}1^+$ $F4/80^-$ leukocytes that respond to acute HSV-1 infection in the cornea.

The early T-cell response to acute HSV-1 infection is not compromised by MDSC in $Kit^{W\text{-}sh}$ mice relative to WT in vivo or in vitro. While we do not contest the significance of MDSC in modulating adaptive responses to chronic conditions, our data using an acute HSV-1 infection model corroborate the findings of Norris et al.,[70] which show that MDSC do not suppress T-cell function during acute viral infection but actively suppress virus-specific T cells and impair the adaptive immune response during the chronic stage of lymphocytic choriomeningitis virus (LCMV) infection.

The enhanced susceptibility of $Kit^{W\text{-}sh}$ mice in our corneal HSV-1 infection model is likely but not exclusively due to enhanced PMN influx resulting from increased permeability of the vasculature. The phenotype manifested in the $Kit^{W\text{-}sh}$ mice is temporal such that by D7 pi, equivalent amounts of virus are recovered in the cornea of WT and $Kit^{W\text{-}sh}$ mice. Such a finding is consistent with the presence of nucleic acid sensors and IFN-α/β–signaling pathways in the cornea that are intimately associated with detection and control of HSV-1.[28,31,71–73] In conclusion, MCs should no longer be considered a harbinger of misery during allergy season but rather a welcome companion in the local ocular mucosal innate immune defense against a common eye pathogen, HSV-1.

Acknowledgments

The authors thank Mark Dittmar and the DMEI Vivarium staff for their help in maintaining our animals, Helen Rosenberg, PhD, for the original source of $CD118^{-/-}$ mice, Doug Drevets, MD, for providing a cytospin centrifuge, Xiaowu "Andy" Gu and Roger Astley for methodologic guidance, and Meghan Carr and Jeremy Jinkins for technical assistance.

Supported by grants from National Institutes of Health R01 EY021238 (DJJC; Bethesda, MD, USA). Additional support includes a senior investigator award from Research to Prevent Blindness (New York, NY, USA) and Presbyterian Health Foundation Presidential Professor Award (DJJC; Oklahoma City, OK, USA), and National Eye Institutes Core Grant EY021725 (Bethesda, MD, USA). DJR is supported by T32EY023202 (Bethesda, MD, USA).

Disclosure: **D.J. Royer**, None; **M. Zheng**, None; **C.D. Conrady**, None; **D.J.J. Carr**, None

References

1. Conrady CD, Drevets DA, Carr DJJ. Herpes simplex type I (HSV-1) infection of the nervous system: is an immune response a good thing? *J Neuroimmunol*. 2010;220:1–9.
2. Duan R, Vries RD de, Osterhaus ADME, Remeijer L, Verjans GM. Acyclovir-resistant corneal HSV-1 isolates from patients with herpetic keratitis. *J Infect Dis*. 2008;198:659–663.
3. Farooq AV, Shukla D. Herpes simplex epithelial and stromal keratitis: an epidemiologic update. *Surv Ophthalmol*. 2012; 57:448–462.
4. Bradley H, Markowitz LE, Gibson T, McQuillan GM. Seroprevalence of herpes simplex virus types 1 and 2—United States, 1999–2010. *J Infect Dis*. 2014;209:325–333.
5. Inoue H, Motani-Saitoh H, Sakurada K, et al. Detection of varicella-zoster virus DNA in 414 human trigeminal ganglia from cadavers by the polymerase chain reaction: a comparison of the detection rate of varicella-zoster virus and herpes simplex virus type 1. *J Med Virol*. 2010;82:345–349.

6. Khanna KM, Lepisto AJ, Hendricks RL. Immunity to latent viral infection: many skirmishes but few fatalities. *Trends Immunol*. 2004;25:230–234.
7. Farooq AV, Valyi-Nagy T, Shukla D. Mediators and mechanisms of herpes simplex virus entry into ocular cells. *Curr Eye Res*. 2010;35:445–450.
8. Conrady CD, Zheng M, Mandal NA, van Rooijen N, Carr DJJ. IFN-α-driven CCL2 production recruits inflammatory monocytes to infection site in mice. *Mucosal Immunol*. 2013;6:45–55.
9. Ambati BK, Nozaki M, Singh N, et al. Corneal avascularity is due to soluble VEGF receptor-1. *Nature*. 2006;443:993–997.
10. Wuest TR, Carr DJJ. The role of chemokines during herpes simplex virus-1 infection. *Front Biosci*. 2008;13:4862–4872.
11. Tumpey TM, Cheng H, Yan XT, Oakes JE, Lausch RN. Chemokine synthesis in the HSV-1-infected cornea and its suppression by interleukin-10. *J Leukoc Biol*. 1998;63:486–492.
12. Kenchegowda S, Bazan HEP. Significance of lipid mediators in corneal injury and repair. *J Lipid Res*. 2010;51:879–891.
13. Wojtasiak M, Pickett DL, Tate MD, et al. Depletion of Gr-1+, but not Ly6G+, immune cells exacerbates virus replication and disease in an intranasal model of herpes simplex virus type 1 infection. *J Gen Virol*. 2010;91(pt 9):2158–2166.
14. Wojtasiak M, Pickett DL, Tate MD, et al. Gr-1+ cells, but not neutrophils, limit virus replication and lesion development following flank infection of mice with herpes simplex virus type-1. *Virology*. 2010;407:143–151.
15. Frank GM, Buela K-AG, Maker DM, Harvey SAK, Hendricks RL. Early responding dendritic cells direct the local NK response to control herpes simplex virus 1 infection within the cornea. *J Immunol*. 2012;188:1350–1359.
16. Smelser GK, Silver S. The distribution of mast cells in the normal eye. *Exp Eye Res*. 1963;2:134–140.
17. Urb M, Sheppard DC. The role of mast cells in the defence against pathogens. *PLoS Pathog*. 2012;8:e1002619.
18. Abraham SN, St John AL. Mast cell-orchestrated immunity to pathogens. *Nat Rev Immunol*. 2010;10:440–452.
19. Wernersson S, Pejler G. Mast cell secretory granules: armed for battle. *Nat Rev Immunol*. 2014;14:478–494.
20. Miller HRP, Pemberton AD. Tissue-specific expression of mast cell granule serine proteinases and their role in inflammation in the lung and gut. *Immunology*. 2002;105:375–390.
21. Jahanyar J, Koerner MM, Loebe M, Youker KA, Torre-Amione G, Noon GP. The role of mast cells after solid organ transplantation. *Transplantation*. 2008;85:1365–1371.
22. Fijak M, Meinhardt A. The testis in immune privilege. *Immunol Rev*. 2006;213:66–81.
23. Anderson DF, Macleod JDA, Baddeley SM, et al. Seasonal allergic conjunctivitis is accompanied by increased mast cell numbers in the absence of leucocyte infiltration. *Clin Exp Allergy*. 1997;27:1060–1066.
24. Williams RM, Singh J, Sharkey KA. Innervation and mast cells of the rat exorbital lacrimal gland: the effects of age. *J Auton Nerv Syst*. 1994;47:95–108.
25. Iwamoto T, Smelser GK. Electron microscope studies on the mast cells and blood and lymphatic capillaries of the human corneal limbus. *Invest Ophthalmol*. 1965;4:815–834.
26. Tharp MD, Seelig LL Jr, Tigelaar RE, Bergstresser PR. Conjugated avidin binds to mast cell granules. *J Histochem Cytochem*. 1985;33:27–32.
27. Li X, Gu X, Boyce TM, et al. Caveolin-1 increases proinflammatory chemoattractants and blood-retinal barrier breakdown but decreases leukocyte recruitment in inflammation. *Invest Ophthalmol Vis Sci*. 2014;55:6224–6234.
28. Conrady CD, Zheng M, Fitzgerald KA, Liu C, Carr DJJ. Resistance to HSV-1 infection in the epithelium resides with the novel innate sensor, IFI-16. *Mucosal Immunol*. 2012;5:173–183.
29. Feduchi E, Carrasco L. Mechanism of inhibition of HSV-1 replication by tumor necrosis factor and interferon gamma. *Virology*. 1991;180:822–825.
30. Sharif NA, Wiernas TK, Griffin BW, Davis TL. Pharmacology of [3H]-pyrilamine binding and of the histamine-induced inositol phosphates generation, intracellular Ca2+-mobilization and cytokine release from human corneal epithelial cells. *Br J Pharmacol*. 1998;125:1336–1344.
31. Wuest T, Austin BA, Uematsu S, et al. Intact TRL 9 and type I interferon signaling pathways are required to augment HSV-1 induced corneal CXCL9 and CXCL10. *J Neuroimmunol*. 2006;179:46–52.
32. Matsuba-Kitamura S, Yoshimoto T, Yasuda K, et al. Contribution of IL-33 to induction and augmentation of experimental allergic conjunctivitis. *Int Immunol*. 2010;22:479–489.
33. Alves-Filho JC, Sônego F, Souto FO, et al. Interleukin-33 attenuates sepsis by enhancing neutrophil influx to the site of infection. *Nat Med*. 2010;16:708–712.
34. Roy A, Ganesh G, Sippola H, et al. Mast cell chymase degrades the alarmins heat shock protein 70, biglycan, HMGB1, and interleukin-33 (IL-33) and limits danger-induced inflammation. *J Biol Chem*. 2014;289:237–250.
35. Doener F, Michel A, Reuter S, et al. Mast cell-derived mediators promote murine neutrophil effector functions. *Int Immunol*. 2013;25:553–561.
36. Nigrovic PA, Gray DHD, Jones T, et al. Genetic inversion in mast cell-deficient (Wsh) mice interrupts corin and manifests as hematopoietic and cardiac aberrancy. *Am J Pathol*. 2008;173:1693–1701.
37. Gabrilovich DI, Nagaraj S. Myeloid-derived suppressor cells as regulators of the immune system. *Nat Rev Immunol*. 2009;9:162–174.
38. Michel A, Schüler A, Friedrich P, et al. Mast cell-deficient Kit(W-sh) "Sash" mutant mice display aberrant myelopoiesis leading to the accumulation of splenocytes that act as myeloid-derived suppressor cells. *J Immunol*. 2013;190:5534–5544.
39. Mantelli F, Calder VL, Bonini S. The anti-inflammatory effects of therapies for ocular allergy. *J Ocul Pharmacol Ther*. 2013;29:786–793.
40. Xu X, Zhang D, Zhang H, et al. Neutrophil histamine contributes to inflammation in mycoplasma pneumonia. *J Exp Med*. 2006;203:2907–2917.
41. Chazot PL. Histamine pharmacology: four years on. *Br J Pharmacol*. 2013;170:1–3.
42. Cíž M, Lojek A. Modulation of neutrophil oxidative burst via histamine receptors. *Br J Pharmacol*. 2013;170:17–22.
43. Tumpey TM, Chen SH, Oakes JE, Lausch RN. Neutrophil-mediated suppression of virus replication after herpes simplex virus type 1 infection of the murine cornea. *J Virol*. 1996;70:898–904.
44. Piliponsky AM, Chen C-C, Rios EJ, et al. The chymase mouse mast cell protease 4 degrades TNF, limits inflammation, and promotes survival in a model of sepsis. *Am J Pathol*. 2012;181:875–886.
45. Hayashi T, Yao S, Crain B, et al. Mast cell-mediated inhibition of abdominal neutrophil inflammation by a PEGylated TLR7 ligand. *Mediators Inflamm*. 2012;2012:262394.

Investigative Ophthalmology & Visual Science

46. Stock AT, Smith JM, Carbone FR. Type I IFN suppresses Cxcr2 driven neutrophil recruitment into the sensory ganglia during viral infection. *J Exp Med*. 2014;211:751–759.
47. Dietrich N, Rohde M, Geffers R, et al. Mast cells elicit proinflammatory but not type I interferon responses upon activation of TLRs by bacteria. *Proc Natl Acad Sci U S A*. 2010; 107:8748–8753.
48. Reichel CA, Rehberg M, Lerchenberger M, et al. Ccl2 and Ccl3 mediate neutrophil recruitment via induction of protein synthesis and generation of lipid mediators. *Arterioscler Thromb Vasc Biol*. 2009;29:1787–1793.
49. Xue M-L, Thakur A, Cole N, et al. A critical role for CCL2 and CCL3 chemokines in the regulation of polymorphonuclear neutrophils recruitment during corneal infection in mice. *Immunol Cell Biol*. 2007;85:525–531.
50. Lundstrom SL, Saluja R, Adner M, Haeggstrom JZ, Nilsson G, Wheelock CE. Lipid mediator metabolic profiling demonstrates differences in eicosanoid patterns in two phenotypically distinct mast cell populations. *J Lipid Res*. 2013;54:116–126.
51. Rajasagi NK, Reddy PBJ, Suryawanshi A, Mulik S, Gjorstrup P, Rouse BT. Controlling herpes simplex virus-induced ocular inflammatory lesions with the lipid-derived mediator resolvin E1. *J Immunol*. 2011;186:1735–1746.
52. Lee J-E, Sun Y, Gjostrup P, Pearlman E. Inhibition of corneal inflammation by the resolvin E1. *Invest Ophthalmol Vis Sci*. 2015;56:2728–2736.
53. Schwab JM, Chiang N, Arita M, Serhan CN. Resolvin E1 and protectin D1 activate inflammation-resolution programmes. *Nature*. 2007;447:869–874.
54. Serhan CN. Pro-resolving lipid mediators are leads for resolution physiology. *Nature*. 2014;510:92–101.
55. Mayer-Barber KD, Andrade BB, Oland SD, et al. Host-directed therapy of tuberculosis based on interleukin-1 and type I interferon crosstalk. *Nature*. 2014;511:99–103.
56. Pazos MA, Pirzai W, Yonker LM, Morisseau C, Gronert K, Hurley BP. Distinct cellular sources of hepoxilin A3 and leukotriene B4 are used to coordinate bacterial-induced neutrophil transepithelial migration. *J Immunol*. 2015;194: 1304–1315.
57. Mrsny RJ, Gewirtz AT, Siccardi D, et al. Identification of hepoxilin A3 in inflammatory events: a required role in neutrophil migration across intestinal epithelia. *Proc Natl Acad Sci U S A*. 2004;101:7421–7426.
58. Srinivasan BD, Kulkarni PS. The role of arachidonic acid metabolites in the mediation of the polymorphonuclear leukocyte response following corneal injury. *Invest Ophthalmol Vis Sci*. 1980;19:1087–1093.
59. Birkle DL, Sanitato JJ, Kaufman HE, Bazan NG. Arachidonic acid metabolism to eicosanoids in herpes virus-infected rabbit cornea. *Invest Ophthalmol Vis Sci*. 1986;27:1443–1446.
60. Sarashina H, Tsubosaka Y, Omori K, et al. Opposing immunomodulatory roles of prostaglandin D2 during the progression of skin inflammation. *J Immunol*. 2014;192:459–465.
61. Rajakariar R, Hilliard M, Lawrence T, et al. Hematopoietic prostaglandin D2 synthase controls the onset and resolution of acute inflammation through PGD2 and 15-deoxy 12-14 PGJ2. *Proc Natl Acad Sci U S A*. 2007;104:20979–20984.
62. Zarbock A, Distasi MR, Smith E, et al. Improved survival and reduced vascular permeability by eliminating or blocking 12/ 15-lipoxygenase in mouse models of acute lung injury (ALI). *J Immunol*. 2009;183:4715–4722.
63. Rossaint J, Nadler JL, Ley K, Zarbock A. Eliminating or blocking 12/15-lipoxygenase reduces neutrophil recruitment in mouse models of acute lung injury. *Crit Care*. 2012;16:R166.
64. Murata T, Aritake K, Matsumoto S, et al. Prostagladin D2 is a mast cell-derived antiangiogenic factor in lung carcinoma. *Proc Natl Acad Sci U S A*. 2011;108:19802–19807.
65. Murata T, Aritake K, Tsubosaka Y, et al. Anti-inflammatory role of PGD2 in acute lung inflammation and therapeutic application of its signal enhancement. *Proc Natl Acad Sci U S A*. 2013;110:5205–5210.
66. Carr DJJ, Chodosh J, Ash J, Lane TE. Effect of anti-CXCL10 monoclonal antibody on herpes simplex virus type 1 keratitis and retinal infection. *J Virol*. 2003;77:10037–10046.
67. Pillay J, Tak T, Kamp VM, Koenderman L. Immune suppression by neutrophils and granulocytic myeloid-derived suppressor cells: similarities and differences. *Cell Mol Life Sci*. 2013;70: 3813–3827.
68. Youn J-I, Collazo M, Shalova IN, Biswas SK, Gabrilovich DI. Characterization of the nature of granulocytic myeloid-derived suppressor cells in tumor-bearing mice. *J Leukoc Biol*. 2012; 91:167–181.
69. Tsiganov EN, Verbina EM, Radaeva TV, et al. Gr-1dimCD11b+ immature myeloid-derived suppressor cells but not neutrophils are markers of lethal tuberculosis infection in mice. *J Immunol*. 2014;192:4718–4727.
70. Norris BA, Uebelhoer LS, Nakaya HI, Price AA, Grakoui A, Pulendran B. Chronic but not acute virus infection induces sustained expansion of myeloid suppressor cell numbers that inhibit viral-specific T cell immunity. *Immunity*. 2013;38:309–321.
71. Kumar A, Zhang J, Yu F-SX Toll-like receptor 3 agonist poly(I:C)-induced antiviral response in human corneal epithelial cells. *Immunology*. 2006;117:11–21.
72. Jin X, Qin Q, Chen W, Qu J. Expression of toll-like receptors in the healthy and herpes simplex virus-infected cornea. *Cornea*. 2007;26:847–852.
73. Hara Y, Shiraishi A, Kobayashi T, et al. Alteration of TLR3 pathways by glucocorticoids may be responsible for immunosusceptibility of human corneal epithelial cells to viral infections. *Mol Vis*. 2009;15:937–948.

Investigative Ophthalmology & Visual Science